

Bias deconstructed: Unravelling the scale dependence of halo bias using real space measurements

Aseem Paranjape^{1,2*}, Emiliano Sefusatti^{2,3}, Kwan Chuen Chan⁴, Vincent Desjacques⁴, Pierluigi Monaco^{5,6} & Ravi K. Sheth^{2,7}

¹ *ETH Zürich, Institute for Astronomy, Wolfgang-Pauli-Strasse 27, CH-8093 Zürich – Switzerland*

² *The Abdus Salam International Center for Theoretical Physics, Strada Costiera, 11, Trieste 34151 – Italy*

³ *INAF, Osservatorio Astronomico di Brera, Via Bianchi 46, I-23807 Merate (LC) – Italy*

⁴ *Département de Physique Théorique and Center for Astroparticle Physics (CAP), Université de Genève, 24 quai Ernest Ansermet, CH-1211 Genève – Switzerland*

⁵ *Dipartimento di Fisica - Sezione di Astronomia, Università di Trieste, via Tiepolo 11, I-34131 Trieste – Italy*

⁶ *INAF, Osservatorio Astronomico di Trieste, Via Tiepolo 11, I-34131 Trieste – Italy*

⁷ *Center for Particle Cosmology, University of Pennsylvania, 209 S. 33rd St., Philadelphia, PA 19104 – USA*

19 January 2021

ABSTRACT

We explore the scale dependence of halo bias using real space cross-correlation measurements in N -body simulations and in PINOCCHIO, an algorithm based on Lagrangian Perturbation Theory. Recent work has shown how to interpret such real space measurements in terms of k -dependent bias in Fourier space, and how to remove the k -dependence to reconstruct the k -independent peak-background split halo bias parameters. We compare our reconstruction of the linear bias, which requires no free parameters, with previous estimates from N -body simulations which were obtained directly in Fourier space at large scales, and find very good agreement. Our reconstruction of the quadratic bias is similarly parameter-free, although in this case there are no previous Fourier space measurements to compare with. Our analysis of N -body simulations explicitly tests the predictions of the excursion set peaks (ESP) formalism of Paranjape et al. (2013) for the scale dependence of bias; we find that the ESP predictions accurately describe our measurements. In addition, our measurements in PINOCCHIO serve as a useful, successful consistency check between PINOCCHIO and N -body simulations that is not accessible to traditional measurements.

Key words: large-scale structure of Universe

1 INTRODUCTION

Galaxies, and the dark matter halos they live in, cluster differently from the underlying dark matter field itself. This halo bias is expected to be nonlinear, nonlocal and stochastic, and understanding its behaviour is a prerequisite to a successful program of precision cosmology with large scale structure. While this nonlinearity, nonlocality and stochasticity of bias is measured in N -body simulations of cold dark matter, its precise physical origin remains unclear, and is likely to be influenced by several effects (Desjacques et al., 2010; Chan, Scocci-

marro & Sheth, 2012; Baldauf et al., 2012; Sheth, Chan & Scoccimarro, 2013). In practice, in the absence of accurate analytical predictions of the so-called nonlinear bias parameters b_n discussed below, one resorts to fitting these parameters to measurements in N -body simulations (Tinker et al., 2005; Pollack, Smith & Porciani, 2012) or marginalising over them when analysing data from galaxy surveys (e.g., Blake et al., 2011; Sánchez et al., 2012), leading to a potential source of unmodelled systematic effects when attempting to recover information on cosmological parameters.

The language used when discussing halo bias is also not unique. Traditional measurements of bias in simulations are performed in Fourier space. For example, “linear

* Email: aseemp@phys.ethz.ch

bias” is typically defined using ratios of power spectra of the halo overdensity $\delta_h(\vec{k})$ and matter overdensity $\delta(\vec{k})$. E.g.,

$$b_1^2(k) \equiv \frac{P_{hh}(k)}{P_{mm}(k)} \quad \text{or} \quad b_1(k) \equiv \frac{P_{hm}(k)}{P_{mm}(k)}, \quad (1)$$

where $P_{hh}(k) = \langle \delta_h^2 \rangle$, $P_{mm}(k) = \langle \delta^2 \rangle$ are halo and matter auto-power spectra, respectively, and $P_{hm}(k) = \langle \delta_h \delta \rangle$ is the corresponding cross-power spectrum. These ratios are found to be scale-independent at large scales (small k) as expected from peak-background split arguments (Kaiser, 1984; Mo & White, 1996; Sheth & Tormen, 1999).

Quadratic bias is typically estimated by measuring (cross-)bispectra of $\delta_h(\vec{k})$ and $\delta(\vec{k})$ and modelling them, e.g., by using perturbation theory or halo model arguments combined with a “local biasing” scheme $\delta_h(\vec{x}) = b_1 \delta(\vec{x}) + b_2 \delta(\vec{x})^2/2! + \dots$ (Fry & Gaztañaga, 1993), and in this case the state-of-the-art (Pollack et al., 2012) shows systematic effects associated with, e.g., shot-noise modelling.

The corresponding real space measurements of bias typically involve gridding the halo and matter density fields on some smoothing scale and then fitting a quadratic relation to the associated scatter plot (e.g., Manera & Gaztañaga, 2012). The resulting fits show a dependence on smoothing scale, although it is not easy to interpret this scale dependence in terms of a k -dependence in Fourier space (Chan & Scoccimarro, 2012). (See also Angulo, Baugh & Lacey, 2008, for a large-scale real-space treatment that assumes local biasing and recovers scale-independent bias parameters to fourth order.)

Recent work using an excursion set approach to the problem has revealed several features of halo bias: (a) Lagrangian Fourier-space bias at any nonlinear order is very naturally linked to a particular real-space definition of Lagrangian bias based on cross-correlating the halo density with a suitable transform of the smoothed initial matter density (Paranjape & Sheth, 2012a; Musso, Paranjape & Sheth, 2012); (b) the excursion set analysis, as well as its extension to peaks theory (Paranjape & Sheth, 2012b; Paranjape, Sheth & Desjacques, 2013), predicts a specific smoothing-scale dependence of these real-space bias parameters, and hence a specific k -dependence in Fourier space; and (c) this scale dependence can be unravelled to reconstruct the large scale, scale-independent bias coefficients using measurements at a finite intermediate smoothing scale. Ultimately, it is the dependence of these scale-independent coefficients on redshift and halo mass that probes the underlying cosmology.

In this paper we apply these ideas to halos identified in N -body simulations of cold dark matter, as well as halos identified in PINOCCHIO (Monaco et al., 2002, 2013), which is a fast algorithm based on Lagrangian Perturbation Theory which provides positions, velocities and merger histories of dark matter halos. The measurements in the N -body simulations constitute a direct test of the excursion set peaks (ESP) formalism (Paranjape et al.,

2013) which, as we show below, fares very well. The additional measurements in PINOCCHIO then become a very useful (and successful) consistency check between PINOCCHIO and the N -body simulations on the one hand, and between PINOCCHIO and ESP on the other. Taken together, our results constitute a self-consistent test of real-space measurements of linear and quadratic bias with *no* free parameters.

The paper is organised as follows. In section 2 we give details of our simulation data set, including a brief description of the PINOCCHIO algorithm. Section 3 deals with measuring the bias parameters and comparing with theory. We first recapitulate in Section 3.1 the real-space definition of the n^{th} order bias parameters b_n and its relation to Fourier-space definitions such as equation (1). Our measurements and the resulting estimates of b_1 and b_2 from the data are described in Section 3.2. We find that these estimates, which we make at different smoothing scales, are in good agreement with the corresponding (scale-dependent) predictions of the ESP formalism. This agreement is important because the measurements themselves are completely independent of the ESP formalism.

In section 3.3 we use the reconstruction algorithm mentioned above, specifically the version described by Paranjape et al. (2013), to obtain estimates of the scale-independent peak-background split parameters b_{10} and b_{20} from the estimates of b_1 and b_2 . The peak-background split bias parameters defined in the excursion set approach directly probe the halo mass function $f(\delta_c; m)$ through

$$b_{n0} = f^{-1} \left(-\frac{\partial}{\partial \delta_c} \right)^n f, \quad (2)$$

where δ_c is the usual overdensity threshold predicted by spherical collapse (Mo & White, 1996; Sheth & Tormen, 1999).

If the reconstruction works well, then these estimates of b_{n0} should be independent of the smoothing scale at which the b_n were measured; we find that this is indeed the case. The linear bias coefficient b_{10} is also directly probed by the large scale limit of Fourier-space measurements such as equation (1) (Paranjape & Sheth, 2012a). We compare our reconstruction of b_{10} with the Fourier-space large scale fit to N -body simulations provided by Tinker et al. (2010), and find very good agreement. For b_{20} there are no previous N -body measurements we can compare with; a comparison with the ESP prediction (Paranjape et al., 2013) shows good agreement. We conclude in section 4.

We assume a flat Λ -cold dark matter cosmology with Gaussian initial conditions and compute transfer functions using CAMB (Lewis, Challinor & Lasenby, 2000)¹ for two different sets of parameter values: $(\Omega_m, \sigma_8, n_s, h, \Omega_b) = (0.272, 0.81, 0.967, 0.704, 0.0455)$ for the N -body simulations and $(0.25, 0.8, 0.95, 0.7, 0.044)$ for PINOCCHIO.

¹ http://lambda.gsfc.nasa.gov/toolbox/tb_camb_form.cfm

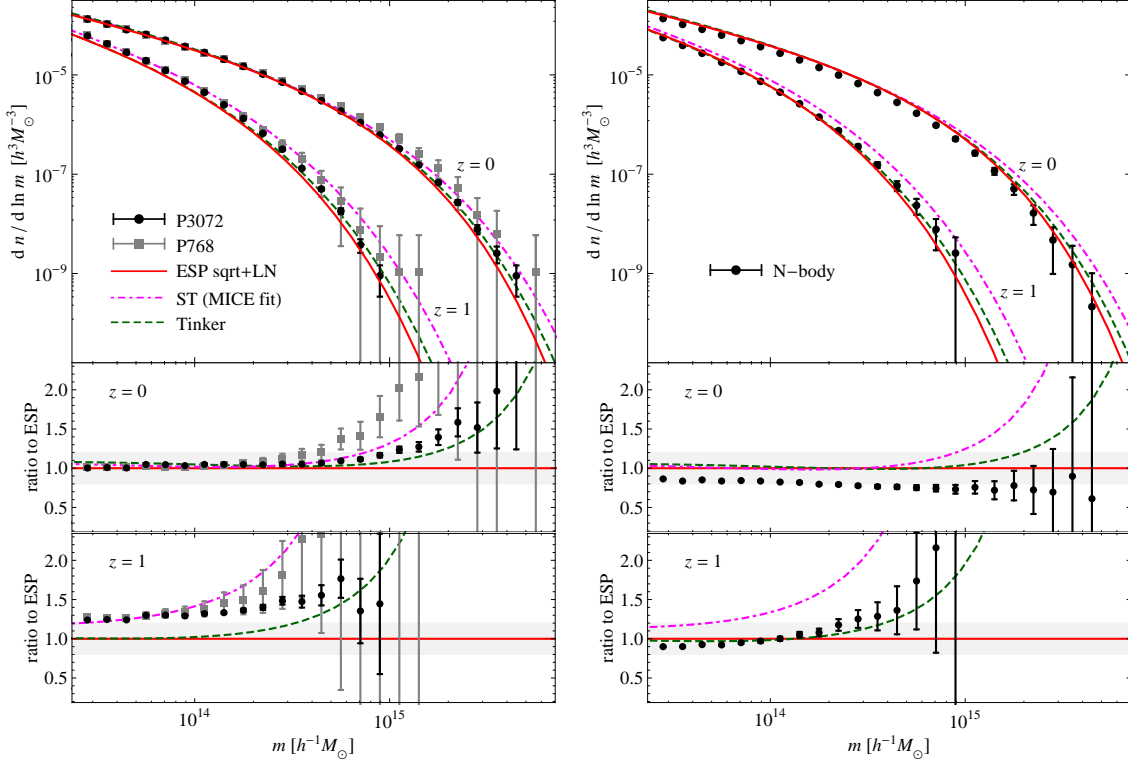


Figure 1. *Left:* Halo mass functions measured in PINOCCHIO using one realization of the 3072 h^{-1} Mpc box (black circles with error bars) and averaged over nine realizations of the 768 h^{-1} Mpc box (gray squares) at redshifts $z = 0$ and $z = 1$. For comparison, the smooth curves show the excursion set peaks (ESP) calculation from Paranjape et al. (2013) (solid red) and two fits to N -body simulations: the fit by Tinker et al. (2008, dashed green) and the Sheth & Tormen (1999) form with their $q = 0.7$ and $p = 0.26$ which we find gives a good fit to the MICE mass function from Crocce et al. (2010, dot-dashed magenta). *Right:* Halo mass functions in our N -body simulations, averaged over six realizations of a 1500 h^{-1} Mpc box (black circles with error bars). The solid curves are the same as in the left panel, but computed using cosmological parameters appropriate for this N -body simulation. See text for a discussion. Lower panels in each case show the ratio of each quantity to the ESP predictions, with the gray band indicating 20% deviations.

2 SIMULATIONS

2.1 N -body

Our cold dark matter simulations were run with 1024^3 particles in a cubic box of size $1500 h^{-1}$ Mpc, with each particle carrying a mass of $2.37 \times 10^{11} h^{-1} M_{\odot}$. Gaussian initial conditions were set at a starting redshift $z = 99$, with initial particle displacements implemented using 2nd order Lagrangian Perturbation Theory (Crocce, Pueblas & Scoccimarro, 2006). The simulations were run using GADGET II (Springel, 2005). We use six realizations, with halos identified using the Spherical Overdensity (SO) halo finder AHF (Gill, Knebe & Gibson, 2004; Knollmann & Knebe, 2009) which uses a redshift-dependent overdensity criterion motivated by spherical collapse (Eke, Cole & Frenk, 1996; Bryan & Norman, 1998). We only study halos having at least 100 particles: this corresponds to halo masses larger than $\sim 10^{13.4} h^{-1} M_{\odot}$.

2.2 PINOCCHIO

For a detailed explanation of the PINOCCHIO code we refer the reader to the original paper and to the more recent Monaco et al. (2013) where its parallel implementation and its application to cosmological volumes are presented. Here we limit ourselves to a quite succinct description.

PINOCCHIO starts from a linear density field generated on a grid in a manner close to the generation of initial conditions in an N -body simulation. It uses 3rd-order LPT applied to the evolution of a homogeneous ellipsoid to compute the collapse times of “particles” (grid points); consistently with the excursion set approach, collapse times are computed for many smoothing radii, thus constructing for each particle a “trajectory” in the plane defined by mass variance and inverse collapse time (the inverse of the growth factor at collapse). At variance with the standard excursion set approach, correlations between trajectories of nearby particles are fully taken into account. An algorithm that mimics the hierarchical assembly of structures is then applied to construct dark matter halos. These are built in the Lagrangian space,

then displaced to their final positions using the Zel'dovich approximation. This algorithm has been tuned to reproduce, to within 5-10%, the “universal” mass function of Warren et al. (2006).

As mentioned above, PINOCCHIO borrows ideas from excursion set theory and, on its own, cannot be considered a completely independent check for the ESP formalism. Nevertheless, these approaches are different enough from each other and from a full-fledged N -body simulation that we believe our analysis provides valuable information on the extent to which each of them reliably captures the underlying physical processes.

We consider here two different set-ups for the PINOCCHIO realizations². The first consists of a box of side $768 h^{-1} \text{Mpc}$ sampled by 1024^3 particles with mass $2.9 \times 10^{10} h^{-1} M_{\odot}$. The second is given instead by a larger box of side $3072 h^{-1} \text{Mpc}$ sampled by 2048^3 particles, each of mass $2.3 \times 10^{11} h^{-1} M_{\odot}$. For the smaller box we produce nine realizations with different initial seeds, in order to provide a more solid estimate of the uncertainties on our results. In each case we only study halos with at least 100 particles.

Monaco et al. (2013) show, using the same realizations, that PINOCCHIO predicts a mass function consistent, within 10%, to the fit of Warren et al. (2006) for the mass range 10^{13} to $10^{15} h^{-1} M_{\odot}$, while a larger discrepancy is observed, in the large mass tail, with the results of Crocce et al. (2010). In addition, for halo populations characterized by a fixed threshold in mass, a 10% agreement is achieved for the linear bias, determined from measurements of the halo-halo power spectrum. Better results for bias are found at lower masses, where the mass function fit is more accurate.

Figure 1 shows the halo mass functions output in these PINOCCHIO realizations (left panels) and measured in our N -body simulations (right panels) at two different redshifts, compared with the fit to N -body simulations by Tinker et al. (2010, specifically, using their SO-200mean parameter values), the Sheth & Tormen (1999, ST) form with their $q = 0.7$ and $p = 0.26$ which we find gives a good fit to the MICE simulations of Crocce et al. (2010), and the analytical ESP calculation from Paranjape et al. (2013). The lower panels in Figure 1 show the ratio of all quantities with the ESP prediction. (We will use a similar format in all our Figures below.) As discussed above, these mass functions agree at the 10-20% level, with larger discrepancies at higher masses. We also note that the halo masses at $z = 0$ in our N -body simulations tend to be $\sim 10\%$ lower than those expected from, e.g., the SO fit by Tinker et al. (2010), and this shows up as a vertical offset in the ratio in the lower panel of the Figure. This could be due to the slightly different halo finding criteria in these simulations; the Tinker et al. (2010) fit we

use corresponds to halos identified by them at a density equal to 200 times the mean density at all redshifts, while the halo finder in our simulation finds halos at $z = 0$ with density ~ 350 times the mean density and at $z = 1$ with ~ 200 times the mean density (Eke et al., 1996; Bryan & Norman, 1998).

3 HALO BIAS IN REAL SPACE

3.1 Analytical motivation

Before presenting our measurements, we summarize our current understanding of halo bias as motivated by the excursion set approach and recapitulate how the reconstruction argument works. This will also serve to set our notation.

Throughout this paper we will focus on Lagrangian bias defined with respect to the linearly extrapolated initial dark matter density field. We will also denote by δ_c the traditional spherical collapse barrier for the excursion set random walks, using³ $\delta_c(z = 0) = 1.686$, and define $\nu \equiv \delta_c / \sqrt{s}$ where

$$s \equiv \sigma_0^2(R) \equiv \langle \delta(R)^2 \rangle = \int d \ln k \Delta^2(k) W(kR)^2 \quad (3)$$

is the linearly extrapolated variance on the Lagrangian scale of the halo, with $\Delta^2(k) \equiv k^3 P(k) / 2\pi^2$ the dimensionless linear matter power spectrum at $z = 0$ and $W(kR)$ the smoothing filter which we will take to be a TopHat in real space so that $W(y) = (3/y^3)(\sin y - y \cos y)$.

Halo bias can be defined in Fourier or real space. E.g., linear bias in Fourier space can be defined using ratios of (cross-)power spectra as in equation (1). While these are convenient definitions, e.g., in an N -body simulation, analytical approaches such as the excursion set formalism work naturally in *real* space, and *a priori* it is not obvious how the results of the latter should be interpreted in Fourier space. Recent work (Paranjape & Sheth, 2012a; Musso & Sheth, 2012; Musso et al., 2012) has shown how this connection can be made in practice. In particular, Musso et al. (2012) argued that a useful definition of the n^{th} order Lagrangian halo bias coefficient b_n in real space is as follows. Consider a simulation in which we have identified halos at some redshift, e.g. $z = 0$. One can now use the particles identified as belonging to a halo in the final nonlinear field to define a “protohalo” in the initial conditions, and compute the

² The two PINOCCHIO runs correspond in size and resolution to the MICE768 and MICE3072 runs of the MICE suite Crocce et al. (2010). This choice is motivated by a direct comparison with those N -body simulations (Monaco et al., 2013)

³ The value 1.686 strictly holds only in an $\Omega_m = 1$ cosmology – we use it primarily for ease of comparison with Paranjape et al. (2013) and Tinker et al. (2010) who also used 1.686. The exact value appropriate for the Λ CDM cosmologies we study would be different from this number at the $\sim 1\%$ level. This would lead to discrepancies in the mass function, at the highest masses, of order 15-20%, whereas in the bias it would cause discrepancies of order $\sim 1\%$ which have no impact on our final results.

center-of-mass of this Lagrangian protohalo using the positions of those same particles in the initial conditions. If there are N halos (equivalently, protohalos) in a given mass bin, then the n^{th} order bias coefficient b_n is estimated at some Lagrangian smoothing scale R_0 as

$$\hat{b}_n = S_0^{-n/2} \frac{1}{N} \sum_{i=1}^N H_n(\delta_{0i}/\sqrt{S_0}), \quad (4)$$

where δ_{0i} is the *dark matter* density contrast in the initial conditions (linearly extrapolated to present epoch) smoothed on the scale R_0 and centered on the center-of-mass in the initial conditions of the i^{th} halo in the bin; S_0 is the linearly extrapolated variance at scale R_0 ,

$$S_0 = \langle \delta_0^2 \rangle = \sigma_0^2(R_0), \quad (5)$$

and the H_n are the probabilist's Hermite polynomials, $H_n(x) = e^{x^2/2}(-d/dx)^n e^{-x^2/2}$, with $p_G(x - \mu; \sigma^2)$ a Gaussian in the variable x with mean μ and variance σ^2 , so that

$$H_1(\delta_0/\sqrt{S_0}) = \frac{\delta_0}{\sqrt{S_0}} \quad \text{and} \quad H_2(\delta_0/\sqrt{S_0}) = \frac{\delta_0^2}{S_0} - 1. \quad (6)$$

The measurement prescription in equation (4) requires the Lagrangian locations of the halos and the corresponding smoothed Lagrangian dark matter overdensities, but is independent of any assumptions specific to a particular excursion set-based prescription such as, e.g., ESP. The motivation for equation (4) is equation (32) of Musso et al. (2012) (see also Szalay, 1988):

$$b_n \equiv \frac{1}{S_0^{n/2}} \langle \rho_h H_n(\delta_0/\sqrt{S_0}) \rangle \\ = \int_{-\infty}^{\infty} d\delta_0 p_G(\delta_0; S_0) \langle \rho_h | \delta_0, S_0 \rangle H_n(\delta_0/\sqrt{S_0}). \quad (7)$$

In the first line, $\rho_h \equiv 1 + \delta_h$ is the normalised Lagrangian halo density field of halos of mass m – essentially, a sum over Dirac delta functions at the appropriate protohalo centers-of-mass discussed above. This formal expression integrates over the distribution of halo-centric R_0 -smoothed δ_0 -values (see Musso et al., 2012, for a discussion of why this distribution is Gaussian to a very good approximation) weighted by the normalised mass fraction $\langle \rho_h | \delta_0, S_0 \rangle = f(m | \delta_0, S_0) / f(m)$ in halos surrounded by a fixed overdensity δ_0 on scale R_0 , which is predicted by the excursion set framework (and, of course, depends on details of the implementation of the latter).

The connection to Fourier-space bias arises as follows. The excursion set analysis (Musso et al., 2012) as well as its ESP extension (Paranjape & Sheth, 2012b; Paranjape et al., 2013) predict the following form⁴ for

⁴ The convention for notation in equation (8) differs from the one used in, e.g., Desjacques et al. (2010). The convention here was introduced by Musso et al. (2012) and is adapted to counting powers of ϵ_\times in real space which roughly correspond to powers of k^2 in Fourier space.

the b_n :

$$b_n = \left(\frac{S_\times}{S_0} \right)^n \sum_{r=0}^n \binom{n}{r} b_{nr} \epsilon_\times^r, \quad (8)$$

where

$$S_\times = \int d \ln k \Delta^2(k) W(kR) W(kR_0), \\ \epsilon_\times = 2 d \ln S_\times / d \ln s \quad (9)$$

are⁵ cross-correlations between the mass overdensity field smoothed on the large scale R_0 and on the Lagrangian scale of the halo $R \propto m^{1/3}$, and the b_{nr} are mass-dependent but scale-independent coefficients whose functional form depends on details of the analysis, such as whether one uses the traditional excursion set calculations of Musso et al. (2012) or the ESP approach of Paranjape et al. (2013).

Among these, the coefficients b_{n0} are somewhat special because they are the logarithmic derivatives of the halo mass function $f(\delta_c, s)$ (Musso et al., 2012) and coincide with the peak-background split bias parameters from equation (2). These are the coefficients one is typically interested in measuring, since they carry information regarding the growth of large scale structure and are hence sensitive to the underlying cosmology. The other coefficients follow from the cross-correlation calculations advocated by Musso et al. (2012); e.g., for $n = 1, 2$ in the ESP case they can be read off from equations (29) and (30) in Paranjape et al. (2013, also see below).

Musso et al. (2012) showed how the appearance of ϵ_\times in the expression for real-space bias signals a k -dependence in Fourier-space bias. Essentially, this is because the real-space cross-correlation that defines b_n can be interpreted in Fourier space by formally introducing $\rho_h(\vec{k})$ and then matching terms in Fourier space with the quantities appearing in equation (8). Roughly, each power of ϵ_\times in real space corresponds to a power of $d \ln W(kR) / d \ln R$ in Fourier space. So, for example, if $W(kR)$ were a Gaussian filter $W(kR) = e^{-k^2 R^2/2}$ then the real-space linear bias $b_1 = (S_\times/S_0)(b_{10} + \epsilon_\times b_{11})$ would translate in Fourier space as $b_1(k) = b_{10} + (k^2 s / \sigma_1^2) b_{11}$ where $\sigma_1^2 = \int d \ln k \Delta^2(k) k^2 e^{-k^2 R^2/2}$. Musso et al. (2012) gave a formal proof that the real-space b_n correspond to integrals over quantities that Matsubara (2012) calls “renormalised” Lagrangian bias coefficients in Fourier space.

A remarkable aspect of the excursion set and ESP frameworks is that there exist linear relations between the b_{nr} which allow *all* of them to be written in terms of

⁵ Strictly speaking, for ESP, ϵ_\times should be defined in terms of mixed spectral moments: $\epsilon_\times = (s/S_\times)(\sigma_{1m\times}^2/\sigma_{1m}^2)$ where $\sigma_{1m}^2 = \int d \ln k \Delta^2(k) k^2 e^{-k^2 R_G^2/2} W(kR)$; $\sigma_{1m\times}^2 = \int d \ln k \Delta^2(k) k^2 e^{-k^2 R_G^2/2} W(kR_0)$ and R_G is matched to R by demanding $\langle \delta_G \delta \rangle = s$ for the reasons discussed by Paranjape et al. (2013). While we implement this in our analysis, we have found that using the second equation in (9) leads to practically identical results.

only the coefficients b_{n0} . E.g., for the simplified case of a constant excursion set barrier $B = \delta_c$, one finds (Musso et al., 2012)

$$\begin{aligned}\delta_c b_{11} &= \nu^2 - \delta_c b_{10} \\ \delta_c^2 b_{21} &= \nu^2 (\delta_c b_{10} - 1) - \delta_c^2 b_{20} \\ \delta_c^2 b_{22} &= \delta_c^2 b_{20} + \nu^2 (\nu^2 - 2\delta_c b_{10} + 1).\end{aligned}\quad (10)$$

This means that the scale dependent coefficients b_1 and b_2 can be written as *linear* combinations of b_{10} and b_{20} . And upon measuring b_1 and b_2 , one can read off the values of b_{10} and b_{20} . This is the basis of the reconstruction procedure proposed by Musso et al. (2012), and generalises to arbitrary order b_{n0} .

There is one complication, though. Paranjape et al. (2013) discussed the fact that the barrier appropriate for the excursion set random walks which determine halo masses is not deterministic, but has a mass-dependent scatter, and argued that this is a key ingredient in the analysis if one demands $\sim 10\%$ accuracy when comparing the halo mass function with that measured in simulations. They showed, based on the N -body results of Robertson et al. (2009), that a good model for this barrier is

$$B = \delta_c + \beta\sqrt{s}, \quad (11)$$

where β is a stochastic variable drawn from a Lognormal distribution whose mean and variance are fixed by the Robertson et al. (2009) results to be approximately 0.5 and 0.25, respectively. (The results for halo bias are very insensitive to the exact choice for this distribution; this is reassuring since Despali, Tormen & Sheth, 2013, suggest slightly different values for the mean and variance of this distribution.)

Define the functions

$$\mu_n(\nu, \beta) = \nu^n H_n(\nu + \beta), \quad (12)$$

and their averages over β ,

$$\begin{aligned}\langle \mu_1 | \nu \rangle &= \nu (\nu + \langle \beta | \nu \rangle), \\ \langle \mu_2 | \nu \rangle &= \langle \mu_1^2 | \nu \rangle - \nu^2 \\ &= \nu^2 (\nu^2 - 1 + 2\nu \langle \beta | \nu \rangle + \langle \beta^2 | \nu \rangle),\end{aligned}\quad (13)$$

where

$$\langle \beta^j | \nu \rangle = \frac{\int d\beta p(\beta) f_{\text{ESP}}(\nu | \beta) \beta^j}{\int d\beta p(\beta) f_{\text{ESP}}(\nu | \beta)}, \quad (14)$$

with $f_{\text{ESP}}(\nu | \beta)$ given in equation (13) of Paranjape et al. (2013). (The second line of equation 13 corrects a typo in equation 37 of Paranjape et al., 2013). Then the estimate for the reconstructed b_{10} becomes (equation 35 of Paranjape et al., 2013),

$$\delta_c \hat{b}_{10}(\nu) = \frac{1}{(1 - \epsilon_\times)} \left[\frac{\delta_c \hat{b}_1}{(S_\times/S_0)} - \epsilon_\times \langle \mu_1 | \nu \rangle \right], \quad (15)$$

which is straightforward to implement since each term is either easily measurable or calculable.

For b_{20} , however, they showed that the exact expression for the reconstruction involves a term $\langle b_1 \mu_1 | \nu \rangle$

which is cumbersome to keep track of (although it is in principle measurable in the simulation). They therefore proposed a simplification based on assuming $\langle b_1 \mu_1 | \nu \rangle \rightarrow \langle b_1 | \nu \rangle \langle \mu_1 | \nu \rangle = \hat{b}_1 \langle \mu_1 | \nu \rangle$, in which case the estimate for b_{20} is (their equation 36)

$$\begin{aligned}\delta_c^2 \hat{b}_{20}(\nu) &= \frac{1}{(1 - \epsilon_\times)^2} \left[\frac{\delta_c^2 \hat{b}_2}{(S_\times/S_0)^2} \right. \\ &\quad \left. - 2\epsilon_\times \left(\frac{\delta_c \hat{b}_1}{(S_\times/S_0)} \langle \mu_1 | \nu \rangle - \langle \mu_1^2 | \nu \rangle \right) \right. \\ &\quad \left. - \epsilon_\times (2 - \epsilon_\times) \langle \mu_2 | \nu \rangle \right].\end{aligned}\quad (16)$$

We will make this assumption in what follows, and leave a more detailed analysis of correlations such as $\langle b_1 \mu_1 | \nu \rangle$ to future work.

3.2 Measurements of b_1 and b_2

We now present measurements for the linear and quadratic bias coefficients defined by equation (4) and measured in the N -body and PINOCCHIO runs described in section 2. These measurements, unlike the reconstruction algorithm which we implement in the next subsection, are completely independent of any theoretical input, other than the recognition that weighting by Hermite polynomials (rather than by simple powers of the density field) is the most natural way to define bias factors in a Gaussian random field (Szalay, 1988; Musso et al., 2012).

Figures 2 and 3 show the results for $\delta_c b_1$ as measured by summing equation (4) over the halos identified at $z = 0$ in the N -body simulations and in PINOCCHIO, respectively. The two panels in each Figure correspond to two different smoothing scales R_0 . Figure 3 shows two sets of measurements; the black circles are from the larger simulation box and the gray squares from the smaller box.

For the N -body simulations, the circles in Figure 2 show the mean over 6 runs and the error bars are the scatter around this mean for each bin. Similarly, the squares in Figure 3 show the mean over 9 runs, and the error bars are the scatter around this mean, for the smaller PINOCCHIO box. For the larger PINOCCHIO box, we had a single run, and the corresponding error bars in Figures 2 and 3 reflect Poisson errors for each mass bin. A comparison of the error bars shows that, at small masses, the Poisson errors are very likely underestimating the scatter in any given bin.

These measurements are susceptible to at least two systematic finite volume effects; the first affects smoothing scales that are a significant fraction of the box size (e.g., $R_0 = 90h^{-1}\text{Mpc}$ in the $768h^{-1}\text{Mpc}$ PINOCCHIO box), and the second affects *mass bins* whose Lagrangian radius is comparable to the smoothing scale (e.g., $\log_{10} \nu^2(m, z=0) = 1.4$ or $m \sim 4.5 \times 10^{15} h^{-1} M_\odot$ which has $R \sim 15h^{-1}\text{Mpc}$, with $R_0 = 30h^{-1}\text{Mpc}$). Our choice of $R_0 = 50h^{-1}\text{Mpc}$ tries to minimize these effects, while $R_0 = 90h^{-1}\text{Mpc}$ highlights the first one.

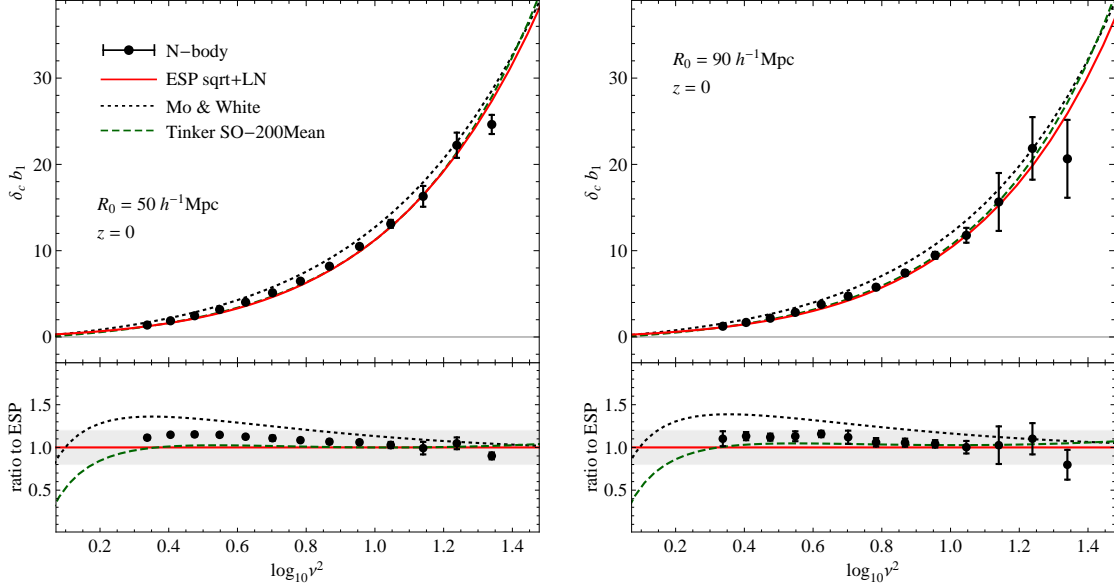


Figure 2. Measurements of the linear halo bias b_1 in the N -body simulations (points with error bars; see text for details). The two panels show measurements at two different smoothing scales. The smooth curves show the corresponding theory predictions using excursion set peaks (solid red) and from Mo & White (1996, dotted black), and the fit to large scale Fourier-space measurements in N -body simulations from Tinker et al. (2010, dashed green). We multiplied the latter two functions with the factor S_\times/S_0 (which slowly varies with mass and is ~ 1.4 for $R_0 = 50h^{-1}\text{Mpc}$ and ~ 1.35 for $R_0 = 90h^{-1}\text{Mpc}$) to account for the mapping from Fourier to real space. The excursion set peaks prediction includes the effect of both S_\times/S_0 as well as ϵ_\times , although the latter effect is quite small at these scales. Lower panels show the ratios with respect to the ESP prediction, with the gray bands indicating 20% deviations.

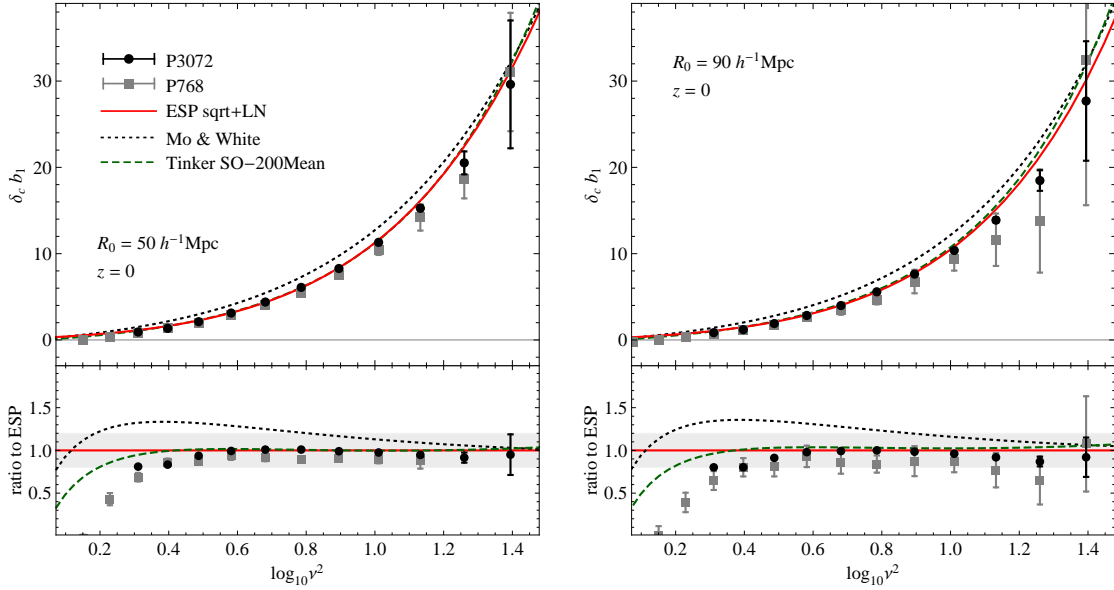


Figure 3. Same as Figure 2, now using measurements in PINOCCHIO. The black circles and gray squares show measurements in the larger and smaller box, respectively. The latter show clear signs of finite volume effects for the larger smoothing scale.

The solid red curves in Figures 2 and 3 are the corresponding predictions of the ESP framework at each smoothing scale (equation 29 of Paranjape et al., 2013), for the respective cosmology. The dashed green lines in each panel are the Lagrangian bias from the fit presented

by Tinker et al. (2010). To be consistent in comparing with our real space measurements, we multiplied this Fourier-space fit with a factor S_\times/S_0 at each smoothing scale. The dotted black curves are the standard spherical collapse prediction $\nu^2 - 1$ (Mo & White, 1996), which

we also multiplied by S_{\times}/S_0 . This is necessary because, although the Mo-White calculation is based on the excursion set approach, it implicitly assumes that the smoothing window with which δ_0 is defined is a TopHat in k -space, for which $S_{\times}/S_0 = 1$, whereas our measurements (along with essentially all other real-space measurements) use a real space TopHat, a point first made by Paranjape & Sheth (2012a).

The careful reader will have noticed that although the dashed and dotted curves are almost the same in the two panels (they differ only because the multiplicative factor S_{\times}/S_0 is about 5% different), the shape of the ESP prediction changes slightly. This is due to the scale dependence introduced by ϵ_{\times} , although this effect is much smaller than the size of the error bars on the measurements. We see that the measurements of b_1 agree very well with the ESP prediction. The small systematic differences between the black circles and the red solid lines in each of the Figures can be traced back entirely to the respective mass functions; the ESP mass function slightly underpredicts the masses of the PINOCCHIO halos and slightly overpredicts those in the N -body simulation (c.f. Figure 1), which is consistent with the trends seen in Figures 2 and 3.

Figures 4 and 5 show the corresponding measurements with errors for the quadratic bias $\delta_c^2 b_2$. The solid red curves in these Figures are the ESP prediction (equation 30 of Paranjape et al., 2013). The dotted black curves are the spherical collapse prediction $\nu^2(\nu^2 - 3)$ (Mo, Jing & White, 1997) multiplied this time by $(S_{\times}/S_0)^2$ to account for the Fourier-to-real-space mapping. In this case there are no previous N -body results to compare with. In addition to the ratios with the ESP prediction in the lower panels, we also show an inset in each plot with a zoomed-in view of the smaller masses.

Once more we find good agreement of the N -body measurements with the ESP prediction (which also appears to be favored over the spherical collapse prediction). Note that the predicted (and measured) values go through zero close to $\log_{10} \nu^2 \simeq 0.6$. This is the first instance of a comparison between a parameter-free measurement of the quadratic bias coefficient b_2 with an analytical prediction, and the agreement we see is very encouraging. The measurements in PINOCCHIO, while in reasonably good agreement with the ESP prediction, appear to show a systematic tendency to lie below the predictions, especially in the right panel of Figure 5. We return to this issue later.

3.3 Reconstructing b_{10} and b_{20}

With the measurements of b_1 and b_2 in hand, we can apply equations (15) and (16) to reconstruct b_{10} and b_{20} , and this requires some theoretical input.

Firstly we must compute the functions S_{\times}/S_0 and ϵ_{\times} which are just integrals over the linear power spectrum (equations 5 and 9, see also footnote 5). A more significant input is the value of the functions $\langle \beta|\nu \rangle$ and $\langle \beta^2|\nu \rangle$ which feed into the algorithm definition through

equation (13). As mentioned earlier, we evaluate these using the ESP prediction $f_{\text{ESP}}(\nu|\beta)$ for the mass fraction at fixed β and a Lognormal distribution for β with mean 0.5 and variance 0.25, the same values used by Paranjape et al. (2013) which were derived from matching to the N -body results of Robertson et al. (2009).

The appearance of $\langle \beta^j|\nu \rangle$ which depends on the ESP mass function means that one cannot interpret the reconstructed \hat{b}_{n0} as clean tests of the ESP formalism. The original reconstruction prescription of Musso et al. (2012) only involved powers of ν (equation 10) rather than integrals over some stochastic variable such as β , so one might argue that their prescription was in some sense cleaner and unaffected by choices regarding, e.g., the choice of distribution $p(\beta)$. This is misleading, however, since that prescription explicitly assumed a constant deterministic barrier which has been shown by Paranjape et al. (2013) to yield a poor description of the halo mass function, which is better described instead by the ingredients discussed above.

The strength of our approach lies in the following. First, our reconstruction below of b_{10} , while model-dependent, agrees very well with the fit presented by Tinker et al. (2010) to large scale *Fourier*-space measurements in N -body simulations. Moreover, this model-dependence is almost entirely driven by the need to describe the mass function accurately (Paranjape et al., 2013), while the prediction for the bias, in a sense, comes for free. Secondly, our reconstruction of b_{20} then makes *no* additional assumptions regarding the underlying model, and is in this sense a parameter-free estimate of quadratic bias. The agreement between the scale-*dependent* measurements of the previous subsection and the corresponding ESP predictions lends support to the expectation that this (albeit model-dependent) reconstruction scheme is correctly capturing the underlying physical processes that lead to halo bias.

The points with error bars in Figure 6 show our reconstruction of $\delta_c b_{10}$ (left panel) and $\delta_c^2 b_{20}$ (right panel) from measurements of b_1 and b_2 in the N -body simulations, for halos identified at $z = 0$, on four different smoothing scales (two of which are the same as in the previous subsection). The errors were calculated by propagating the errors (i.e., scatter around the mean) on b_1 and b_2 . Figure 7 shows the corresponding reconstructions in the $3072 h^{-1} \text{Mpc}$ PINOCCHIO box; in this case the errors were computed by propagating Poisson errors.

We see in the left panel of Figure 6 that the reconstruction of b_{10} at all scales gives nearly identical results (indicating that the algorithm is working well in removing the scale dependence). The reconstructed values are also in good agreement with the fit presented by Tinker et al. (2010, dashed green) and the ESP prediction (solid red; equation 29 of Paranjape et al., 2013, with $\epsilon_{\times} \rightarrow 0$ and $S_{\times}/S_0 \rightarrow 1$), apart from a minor trend caused by the mass mismatch seen in Figure 1. For comparison, we also show the spherical collapse prediction $\nu^2 - 1$ (Mo & White, 1996, dotted black) and the peak-background split prediction associated with the ST fit to the MICE

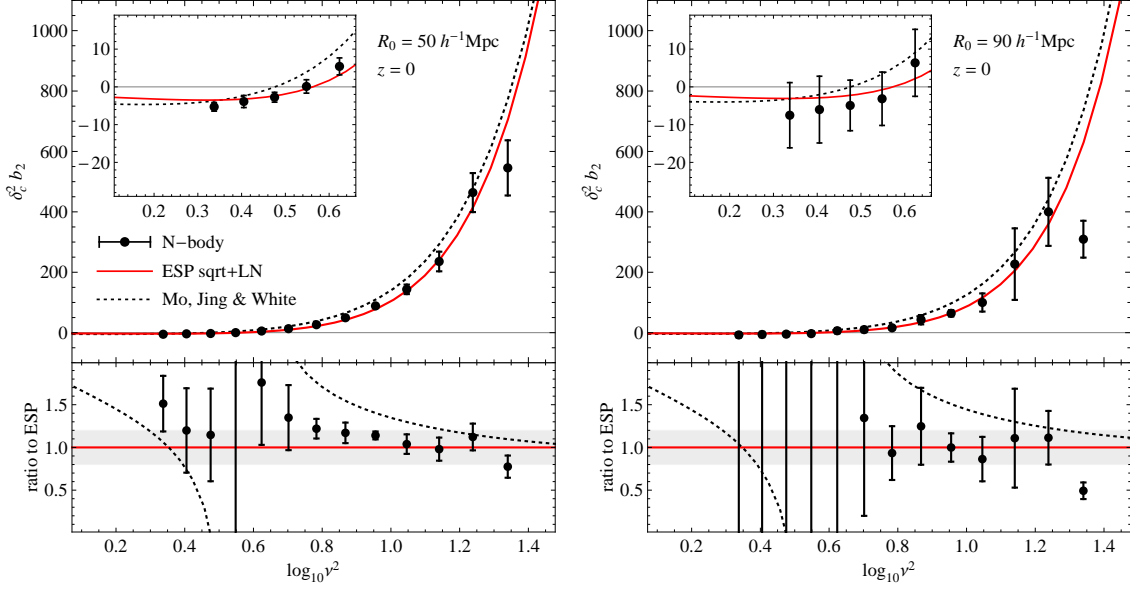


Figure 4. Measurements of the quadratic halo bias b_2 in the N -body simulations (points with error bars; see text for details). The left and right panels show measurements at two different smoothing scales (the same as in Figure 2). The smooth curves show the corresponding theory predictions using excursion set peaks (solid red) and from Mo et al. (1997, dotted black), the latter being multiplied with the factor $(S_\times/S_0)^2$ to account for the mapping from Fourier to real space. In this case there are no prior N -body simulation results to compare with. Insets show zoomed-in views of the lowest masses. Lower panels show the ratios with respect to the ESP prediction, with the gray bands indicating 20% deviations.

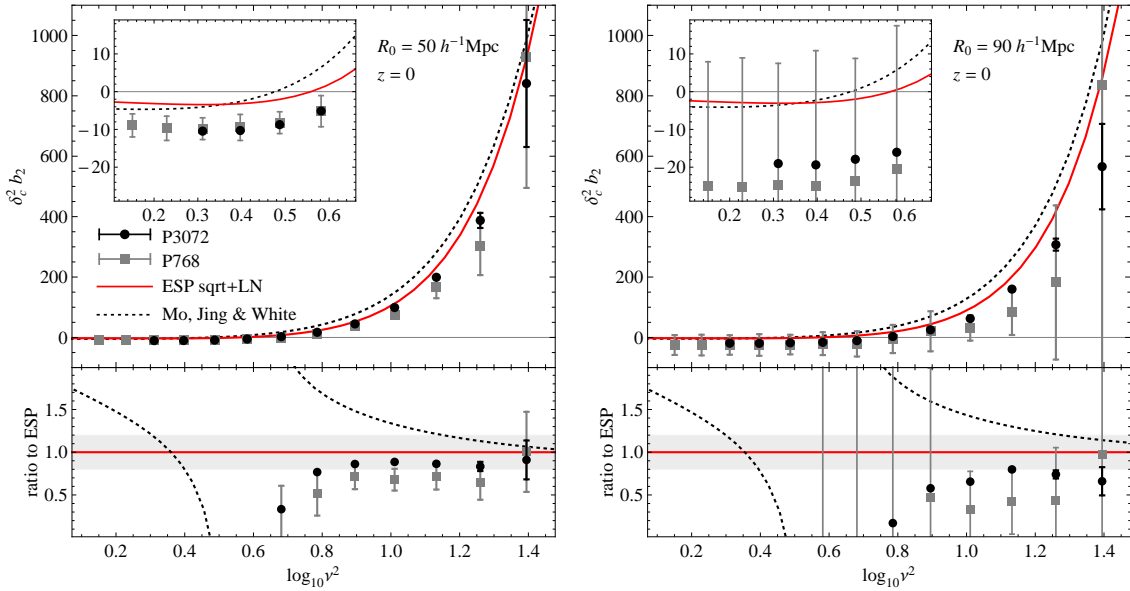


Figure 5. Same as Figure 4, now using measurements in PINOCCHIO. The black circles and gray squares show measurements in the larger and smaller box, respectively. Finite volume effects are apparent at large masses for the measurements in the smaller simulation box.

mass function (the ST mass function in equation 2 with $n = 1$; dot-dashed magenta).

The reconstruction of b_{20} in the right panel of Figure 6 shows similar behaviour, and the measurements at all scales are in reasonable agreement with the ESP prediction (solid red; equation 30 of Paranjape et al., 2013,

with $\epsilon_\times \rightarrow 0$ and $S_\times/S_0 \rightarrow 1$). For comparison, we also show the spherical collapse prediction $\nu^2(\nu^2 - 3)$ (Mo & White, 1996, dotted black) and the peak-background split prediction from the ST fit to the MICE mass function (dot-dashed magenta, the ST mass function in equation 2 with $n = 2$; see also Scoccimarro et al., 2001). In

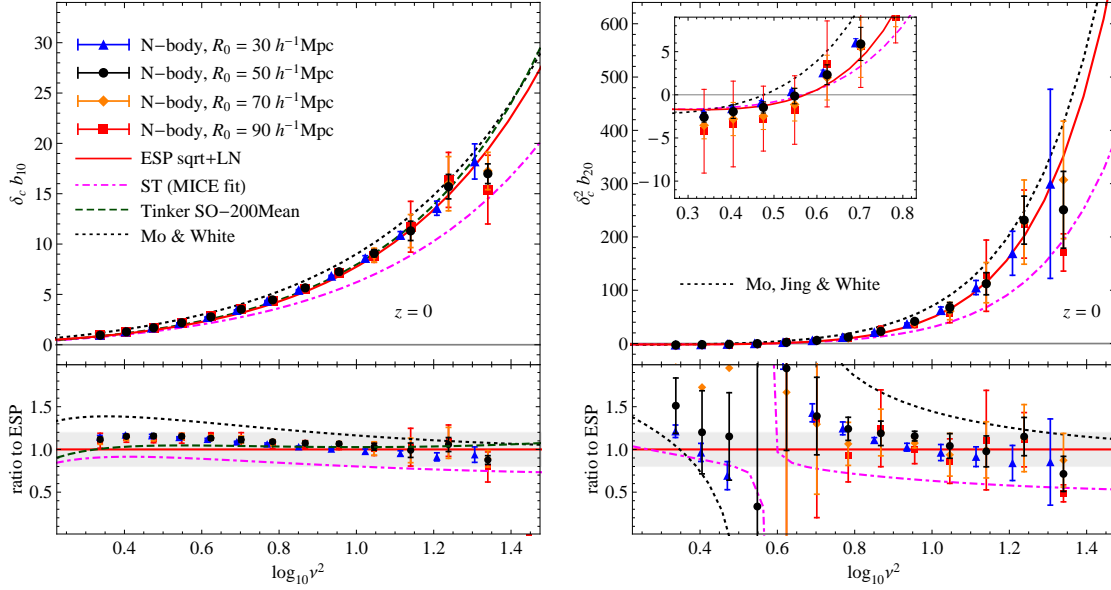


Figure 6. The reconstruction technique described in the text applied to the N -body measurements of linear and quadratic bias at $z = 0$ at four different smoothing scales. *Left:* Reconstructing b_{10} . The measurements are in excellent agreement with each other (indicating that the algorithm is working well) and with the fit to Fourier-space measurements from Tinker et al. (2010, dashed green) as well as the ESP prediction (solid red) apart from a minor trend caused by the mass mismatch seen in Figure 1. For comparison we also show the prediction from Mo & White (1996, dotted black) and the peak-background split prediction using the ST fit to the MICE mass function (the ST mass function with $q = 0.7$, $p = 0.26$ in equation 2 with $n = 1$; dot-dashed magenta). *Right:* Reconstructing b_{20} . The measurements again agree well with each other, although they are noisier than those of b_{10} . The smooth curves show the prediction of ESP (solid red), Mo et al. (1997, dotted black) and the peak-background split prediction from the ST fit to the MICE mass function (dot-dashed magenta, the ST mass function with $q = 0.7$, $p = 0.26$ in equation 2 with $n = 2$). The inset shows a zoom-in of the lowest masses. Note that the predicted values and measurements go through zero close to $\log_{10} \nu^2 \simeq 0.6$. Lower panels in each case show the ratios with respect to the ESP prediction, with the gray bands indicating 20% deviations.

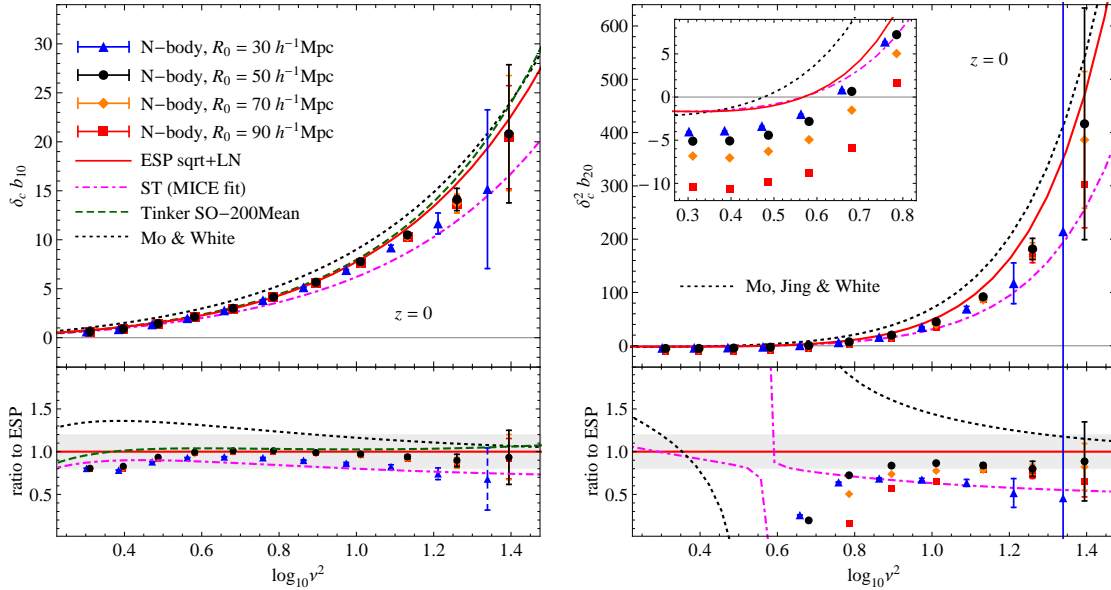


Figure 7. Same as Figure 6, now for the $3072 h^{-1} \text{Mpc}$ PINOCCHIO box at $z = 0$. In the left panel, the b_{10} measurements are in excellent agreement with each other (with some hints of systematic volume effects at $R_0 = 30 h^{-1} \text{Mpc}$) and with the fit to Fourier-space measurements from Tinker et al. (2010, dashed green) as well as the ESP prediction (solid red). In the right panel, the b_{20} measurements show a systematic decrease as R_0 increases.

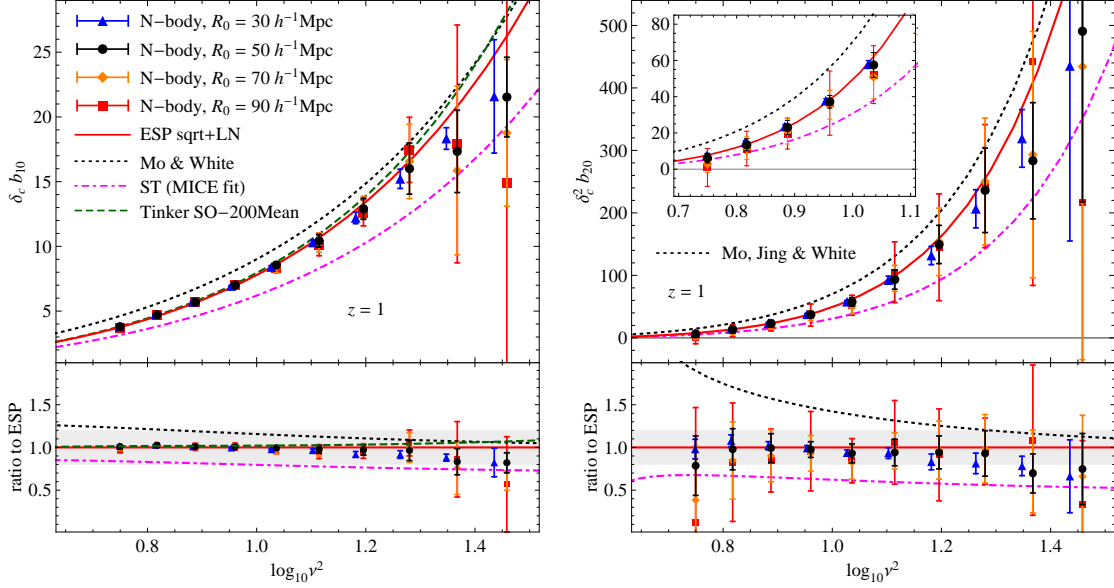


Figure 8. Same as Figure 6, now using halos identified at redshift $z = 1$ in the N -body simulation. The measurements of b_{10} are in excellent agreement with each other and with the Fourier-space fit from Tinker et al. (2010) as well as the ESP prediction. Both b_{10} and b_{20} now display possible sample variance effects at large masses ($\log_{10} \nu^2(m, z = 1) \gtrsim 1.3$, or $m \gtrsim 6 \times 10^{14} h^{-1} M_{\odot}$). See text for a discussion.

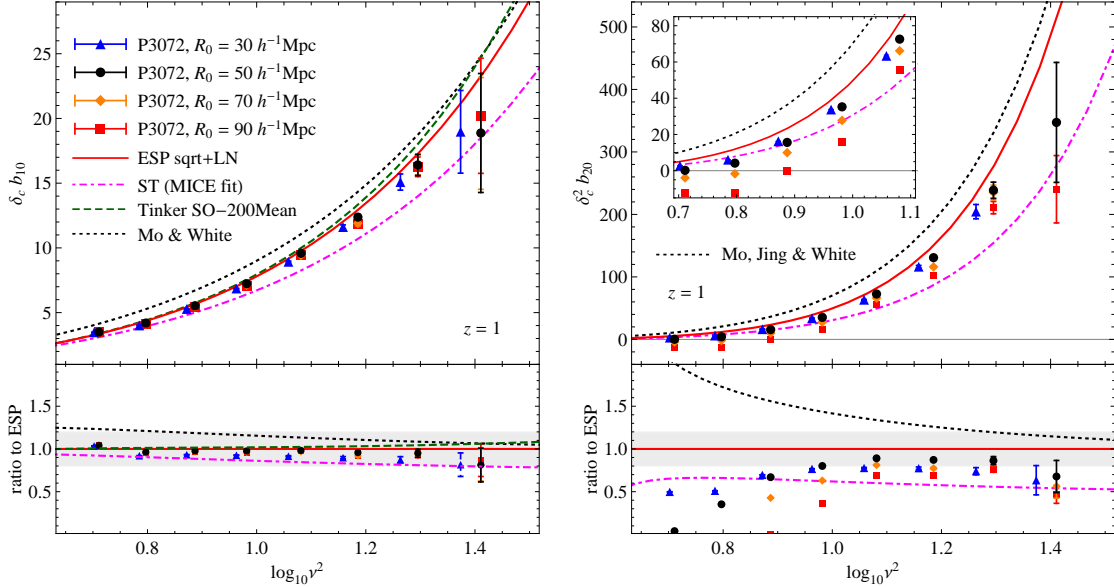


Figure 9. Same as Figure 7, now using halos identified at redshift $z = 1$ in the $3072 h^{-1} \text{Mpc}$ PINOCCHIO box. See text for a discussion.

addition to the ratio with ESP predictions in the lower panels, the b_{20} plot also shows an inset with a zoomed-in view of the lowest masses. Note that the predictions and measurements go through zero close to $\log_{10} \nu^2 \simeq 0.6$.

Correspondingly, the measurements of b_{10} at $z = 0$ in PINOCCHIO (left panel of Figure 7) are also in excellent agreement with each other and with the ESP prediction. In this case, the reconstruction of b_{20} in the right panel, while in reasonable agreement across scales, shows a sys-

tematic tendency towards lower values as R_0 is increased. We have noticed similar trends to a lesser extent in our individual N -body realisations as well (not displayed); these trends are the main reason that the scatter in the b_{20} measurements in the right panel of Figure 6 increases with smoothing scale R_0 . The trend in the right panel of Figure 7 could therefore be due to sample variance.

Figures 8 and 9 have a format identical to Figures 6 and 7, but show results obtained using halos identified

at $z = 1$ in the N -body simulations (Figure 8) and in the larger PINOCCHIO box (Figure 9). Once again, the measurements of b_{10} at different smoothing scales are in excellent agreement with each other and with the Fourier-space fit from Tinker et al. (2010) as well as the ESP prediction. The b_{20} measurements again show a systematic drift in the single PINOCCHIO realisation and a large realisation-to-realisation scatter in the N -body results. Additionally, there seems to be a systematic turnover at high masses ($\log_{10} \nu^2(m, z = 1) \gtrsim 1.3$ or $m \gtrsim 6 \times 10^{14} h^{-1} M_{\odot}$) in both b_{10} and b_{20} at all smoothing scales, which is more pronounced in the N -body simulation than in PINOCCHIO. Since the PINOCCHIO box has more than 8 times the volume of our individual N -body realisations, this is also likely to be a sample variance effect. We discuss other possible sources for these trends in Section 4 below.

4 DISCUSSION

The scale-dependence and nonlinearity of halo bias is a potential source of systematic effects for upcoming galaxy surveys, which can degrade the measurements of cosmological parameters. Current strategies for dealing with these effects mainly rely on using parametrized functions inspired by fits to N -body simulations (Tinker et al., 2005; Pollack et al., 2012). In principle, though, such effects can be modelled using analytical tools such as the excursion set formalism. While such models predict the linear, scale-independent part of halo bias with reasonable accuracy, they have not fared well until now in predicting these “beyond linear” effects.

We have presented real-space measurements of Lagrangian halo bias at linear and quadratic order using a recently proposed technique (Musso et al., 2012; Paranjape et al., 2013) which exploits the correlation between the locations of halo formation in the initial conditions and the large scale initial environment. The “observables” in this measurement – namely, the scale dependent bias coefficients b_n (equation 4) – can be estimated using simple measurements in the initial conditions of a simulation, and are direct predictions of the excursion set peaks (ESP) formalism of Paranjape et al. (2013). We find that our measurements in N -body simulations (Figures 2 and 4) and in the PINOCCHIO algorithm (Figures 3 and 5) are in very good agreement with expectations using ESP.

Further, the ESP formalism also shows how these scale-dependent measurements of b_n can be converted into scale-independent estimates of the peak-background split parameters b_{n0} defined by equation (2). We find good agreement between our estimates of b_{10} in Figures 6, 7, 8 and 9 and the fit to large scale Fourier-space linear bias in N -body simulations presented by Tinker et al. (2010), which represents a success of the ESP formalism. Furthermore, the reconstruction of b_{n0} utilizes no additional assumptions other than those required to obtain a good description of the mass function; in this sense, we have presented a parameter-free prescription

for estimating nonlinear large scale (i.e. small k or large R_0) bias from intermediate scale measurements (we used $R_0 = 30, 50, 70, 90 h^{-1} \text{Mpc}$).

Our analysis and results raise a number of interesting issues that must be addressed to assess and utilize the full potential of our approach:

- We note that our estimates of b_{10} and b_{20} show departures from the theoretical predictions at the largest halo masses; these are especially pronounced in the N -body results at $z = 1$ (Figure 8). As discussed in the text, a likely cause for these is sample variance. Additionally, at small smoothing scales like $R_0 = 30 h^{-1} \text{Mpc}$ the trends could be partly due to the fact that the largest halos have Lagrangian sizes that approach this size. There is also the possibility that nonlocality induced by effects such as those studied by Sheth et al. (2013) could be contaminating our reconstruction algorithm at high masses. It will be interesting to check whether such nonlocal, non-spherical effects can be isolated from the recovery of the b_{n0} , e.g., using the rotational-invariance motivated orthogonal polynomials associated with peak shapes (Gay et al., 2012; Desjacques, 2013) and the tidal field (Sheth et al., 2013). This should require straightforward extensions of our technique to measuring quantities other than the density.

- Another important question is whether our technique, which works at finite scales, can become a realistic, cost-effective method for measuring bias in the *late-time*, gravitationally evolved Eulerian field. We have presented results using smoothing scales $R_0 \geq 30 h^{-1} \text{Mpc}$, which are large compared with, e.g., those used by Angulo et al. (2008) in their Eulerian analysis that recovered bias coefficients up to 4th order. The reason for having these large Lagrangian smoothing scales is simply that the most massive protohalos we work with have Lagrangian sizes that can approach $\sim 15\text{--}20 h^{-1} \text{Mpc}$. Halos in the Eulerian field are much more compact, so in principle our technique should be applicable at much smaller scales in this case. A bigger issue is the fact that the Eulerian field is weakly non-Gaussian, so using Hermite polynomials as we currently do may not be the best approach. Although one can find natural generalisations of the Hermite polynomials appropriate for non-Gaussian fields (e.g., see Appendix B2 of Musso et al., 2012), the question of which basis set to use in extracting nonlinear Eulerian bias is still not fully settled.

- Our original goal included a measurement of the k -dependence of linear bias as implied by the presence of the quantity ϵ_{\times} in the excursion set prediction in equation (8); however, this effect is too small to be reliably seen given our present error bars. For scale-dependent bias in the *Eulerian* field, there is also the related question of whether triaxiality of halos could be a source of significant systematics for our reconstruction technique. The Eulerian field will also be affected by gravitationally induced nonlocality (Chan et al., 2012) which would have to be accounted for.

And finally, it will be very interesting to assess to

what extent a self-consistent estimate of nonlinear and nonlocal halo bias in galaxy surveys can improve the recovery of cosmological parameters. We leave a detailed exploration of all these issues to future work.

ACKNOWLEDGMENTS

We thank Roman Scoccimarro for collaboration in the initial stages of this work, and both him and Marcello Musso for useful discussions. KCC and VD acknowledge support by the Swiss National Science Foundation. RKS is supported in part by NSF-AST 0908241.

References

- Angulo R. E., Baugh C., Lacey C., 2008, MNRAS, 387, 921
- Baldauf T., Seljak U., Desjacques V., McDonald P., 2012, PRD, 86, 083540
- Blake C. et al., 2011, MNRAS, 418, 1707
- Bryan G. L., Norman M. L., 1998, ApJ, 495, 80
- Chan K. C., Scoccimarro R., 2012, PRD, 86, 103519
- Chan K. C., Scoccimarro R., Sheth R. K., 2012, PRD, 85, 083509
- Crocce M., Fosalba P., Castander F. J., Gaztañaga E., 2010, MNRAS, 403, 1353
- Crocce M., Pueblas S., Scoccimarro R., 2006, MNRAS, 373, 369
- Desjacques V., Crocce M., Scoccimarro R., Sheth R. K., 2010, PRD, 82, 103529
- Desjacques V., 2013, PRD, 87, 043505
- Despali G., Tormen G., Sheth R. K., 2013, MNRAS, 431, 1143
- Eke V. R., Cole S., Frenk C. S., 1996, MNRAS, 282, 263
- Fry J. N., Gaztañaga E., 1993, ApJ, 413, 447
- Gay C., Pichon C., Pogosyan D., 2012, Phys Rev D., 85, 023011
- Gill S. P. D., Knebe A., Gibson B. K., 2004, MNRAS, 351, 399
- Kaiser N., 1984, ApJ, 284, L9
- Knollmann S. R., Knebe A., 2009, ApJS, 182, 608
- Lewis A., Challinor A., Lasenby A., 2000, ApJ, 538, 473
- Manera M., Gaztañaga E., 2011, MNRAS, 415, 383
- Matsubara T., 2011, PRD, 83, 083518
- Mo H. J., Jing Y. P., White S. D. M., 1997, MNRAS, 284, 189
- Mo H. J., White S. D. M., 1996, MNRAS, 282, 347
- Monaco P., Theuns T., Taffoni G., 2002, MNRAS, 331, 587
- Monaco P., Sefusatti E., Borgani S., Crocce M., Fosalba P., Sheth R. K., Theuns T., *accepted by* MNRAS
- Musso M., Paranjape A., Sheth R. K., 2012, MNRAS, 427, 3145
- Musso M., Sheth R. K., 2012, MNRAS, 423, 102
- Paranjape A., Sheth R. K., 2012a, MNRAS, 419, 132
- Paranjape A., Sheth R. K., 2012b, MNRAS, 426, 2789
- Paranjape A., Sheth R. K., Desjacques V., 2013, MNRAS, 431, 1503
- Pollack J. E., Smith R. E., Porciani C., 2012, MNRAS, 420, 3469
- Robertson B. E., Kravtsov A. V., Tinker J., Zentner A. R., 2009, ApJ, 696, 636
- Sánchez A. G. et al., 2012, MNRAS, 425, 415
- Scoccimarro R., Sheth R. K., Hui L., Jain B., 2001, ApJ, 546, 20
- Sheth R. K., Tormen G., 1999, MNRAS, 308, 119
- Sheth, R. K., Chan, K. C., Scoccimarro, R., 2013, PRD, 87, 083002
- Springel V., 2005, MNRAS, 364, 1105
- Szalay A., 1988, ApJ, 333, 21
- Tinker J. L., Kravtsov A. V., Klypin A., Abazajian K., Warren M. S., Yepes G., Gottlöber S., Holz D. E., 2008, ApJ, 688, 709
- Tinker J. L., Robertson B. E., Kravtsov A. V., Klypin A., Warren M. S., Yepes G., Gottlöber S., 2010, ApJ, 724, 878
- Tinker, J. L., Weinberg, D. H., Zheng, Z., Zehavi, I. 2005, ApJ, 631, 41
- Warren M. S., Abazajian K., Holz D. E., Teodoro L., 2006, ApJ, 646, 881